SPE/ISRM 78238

Development of an Orthotropic 3D Elastoplastic Material Model for Shale

Anthony J.L. Crook, Jian-Guo Yu (Rockfield Software Ltd.) & Stephen M. Willson (BP America Inc.)

Copyright 2002, Society of Petroleum Engineers Inc.

This paper was prepared for presentation at the SPE/ISRM Rock Mechanics Conference held in Irving, Texas, 20-23 October 2002.

This paper was selected for presentation by an SPE/ISRM Program Committee following review of information contained in an abstract submitted by the author(s). Contents of the paper, as presented, have not been reviewed by the Society of Petroleum Engineers or International Society of Rock Mechanics and are subject to correction by the author(s). The material, as presented, does not necessarily reflect any position of the Society of Petroleum Engineers, International Society of Rock Mechanics, its officers, or members. Papers presented at SPE/ISRM meetings are subject to publication review by Editorial Committees of the Society of Petroleum Engineers. Electronic reproduction, distribution, or storage of any part of this paper for commercial purposes without the written consent of the Society of Petroleum Engineers is prohibited. Permission to reproduce in print is restricted to an abstract of not more than 300 words; illustrations may not be copied. The abstract must contain conspicuous acknowledgment of where and by whom the paper was presented. Write Librarian, SPE, P.O. Box 833836, Richardson, TX 75083-3836, U.S.A., fax 01-972-952-9435.

Abstract

Shales encountered in the overburden above hydrocarbon reservoirs often pose challenges to the stability of boreholes. Consequently, there is a keen interest in borehole stability prediction, which is complicated by the laminated structure of shale that arises as a consequence of the depositional environment.

A combined experimental/numerical investigation is being undertaken to address how the directional properties of shale impact borehole stability in weak shale formations. Within this paper an advanced finite element procedure for simulation of progressive damage of orthotropic pressure-sensitive materials is presented, which includes bifurcation and post-bifurcation analysis. This constitutive model is based on critical state theory and is specifically designed to represent the characteristic deformation of weak shale formations. It includes orthotropic elasticity and an orthotropic pressure-dependent yield surface that is curved in the p-q plane, and which intercepts the hydrostatic axis in both tension and compression. A regularization procedure is also presented that ensures mesh invariance and correctly reproduces the dependence of strength on the size of the test specimen.

Calibration of the model parameters is also discussed and the model is validated by comparison with the results of uniaxial and triaxial compression tests for Pierre I Shale performed at different bedding plane orientations.

Introduction

Despite significant advances in prediction in recent years, wellbore instability can still occur in shales during drilling. While instability in homogeneous shales can largely be avoided by using an adequate mud weight, attention is now focusing on predicting instability in shales with a more pronounced 'fabric' or fissile character. This anisotropy in mechanical and strength properties is usually neglected in conventional analyses. However, shales usually possess a laminated structure as a consequence of the depositional environment, and therefore exhibit a directional variation in elastic properties, yield strength and post-yield behaviour. Conventional approaches – assuming transverse isotropic elastic properties with isotropic failure surfaces – are typically unable to properly reproduce the complex yield and deformation behaviour of these materials. This deficiency is most pronounced in highly laminated and fissile shales, which are the most likely to cause drilling problems. The low permeability of shale may also complicate the stability assessment by necessitating a coupled poroelastic formulation.

Extensive research has been carried out on the formulation of appropriate failure criteria for orthotropic and transversely isotropic materials, see [4] for a recent review. Early work focused on empirical failure criteria that account for the continuous variation of compressive strength with orientation for transversely isotropic rock [5,6]. Subsequently Tsai and Wu [7] and Pariseau [8] extended Hill's criterion [9] for orthotropic metal plasticity to pressure sensitive materials, and Ong and Roegiers [10] employed these theories in horizontal wellbore stability predictions. Nova [11] proposed a generalised failure condition that describes failure of transversely isotropic rocks in compression and Nova and Zaninetti [12] established a failure criterion in tension based on similar concepts. Cazacu and Critescu [13] show that an anisotropic Mises-Schleicher (AMS) criterion can accurately fit the failure strength for transversely isotropic rocks, including the directional character of transversely isotropic materials under general loading conditions, and the dependence on the intermediate principal stress.

The development of a description of the progressive failure for orthotropic and transversely isotropic materials has received less attention, probably due to the complexities associated with the formulation of the problem. Some researchers have adopted the Hoffman criterion [14], a pressure sensitive extension of the Hill criterion with a paraboloid shape in the p-q plane [15]. Also Pietruszczak et al. [16] proposed a formulation that incorporates a scalar anisotropy parameter that is expressed in terms of mixed invariants of stress and structure-orientation tensors. This

model shows good correspondence with the pre-peak response of Tournemire shale but in the form presented the model does not account for the post-peak evolution of the material. Dafalias [17] and Voyiadjis and Song [18] present some theoretical aspects of modelling anisotropic materials with an anisotropic Cam Clay model but focus on texture development rather than materials with inherent initial anisotropy.

An anisotropic constitutive model, formulated by extending the isotropic Modified Cam Clay critical state model for materials with pre-defined structure, is presented in this study. The model includes orthotropic elasticity, an orthotropic pressure dependent yield surface and hardening/softening governed by the evolution of volumetric plastic strain. A regularization procedure, based on fracture mechanics concepts, is also presented. The model is validated by comparison with the results of triaxial compression tests performed at different orientations to bedding in laminated shale. Note that the bedding plane orientation in the triaxial tests is denoted by the angle θ relative to the radial direction (Figure 1).

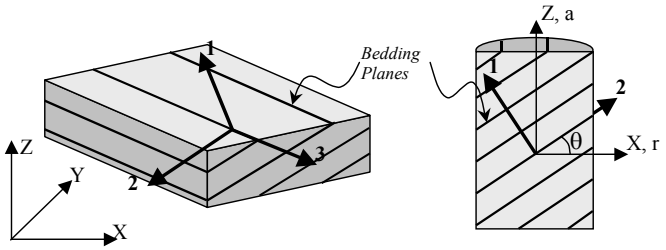

(a) General System *(b) Triaxial System*

Figure 1. Local Coordinate System Aligned with Bedding Planes

Experimentally Observed Characteristics of Shales

Transverse isotropic shales have generally been studied experimentally using triaxial tests subjected to globally axisymmetric loading states, although the true stress states will not be axisymmetric due to bedding plane inclination, inhomogeneities in the specimens and end effects. These studies, for example [1-3], have shown that:

1. The variation of the compressive strength with the angle between the bedding planes and loading direction is such that the maximum compressive strength occurs when the loading direction is either parallel or perpendicular to the bedding planes (Figure 2).
2. The minimum compressive stress occurs when the loading to bedding plane orientation lies between 30° and 60° where the high shear stresses promote failure on the bedding planes (Figure 2).
3. The elastic properties are transverse isotropic, with the Young's modulus normal to the bedding planes being lower than the Young's modulus in the plane of the bedding.
4. The elastic properties are a nonlinear function of confining pressure but also dependent on effective stress.
5. The failure surface is nonlinear in the p-q plane (Figure 3).
6. At low confinement, failure is brittle with a sudden loss in strength and a transition from compressive to dilatant volumetric strain during and post failure (Figure 4).

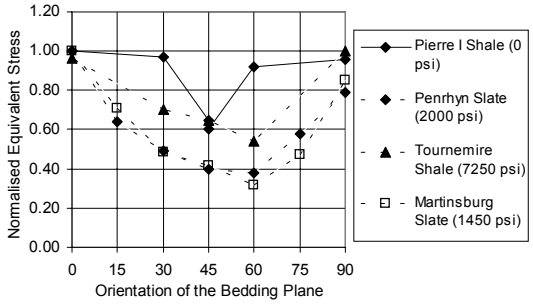

Figure 2. Variation of Normalised Failure Stress with Bedding Plane Orientation

7. At high confinement the deformation of weaker shales remains compressive with no softening once the peak strength is exceeded (Figure 4).
8. Time dependency is important due to the low permeability of shale.

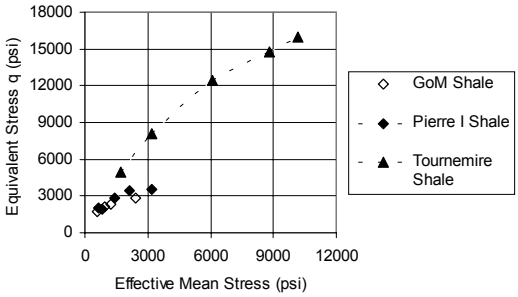

Figure 3. Typical Strength for Shale in the p-q Plane

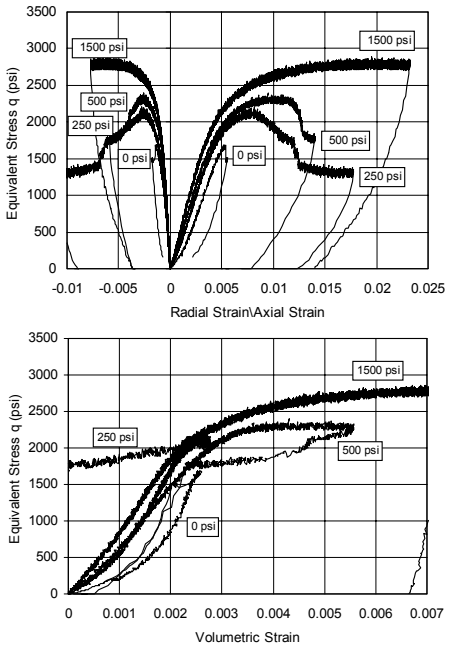

Figure 4. Stress-Strain Curves for Typical GoM Shale

The most extensive set of published laboratory experiments on the influence of anisotropy in shale have been performed on Tournemire shale, an Upper Toarcian massive shale taken from the Tournemire site in the Massif Central, France. Both compressibility and triaxial tests were utilised with the emphasis of evaluating the elastic, yield and failure response as a function of confining pressure and bedding plane orientation. Tournemire shale is, however, moderately strong and therefore not necessarily representative for weaker shales.

Experimental data for weak shales is quite sparse. A short experimental investigation of the influence of bedding plane orientation on failure has therefore been performed on Pierre I shale. This is an Upper Cretaceous, very fine grained, black claystone, with 20 to 30% clay content, that outcrops in eastern Colorado. The formation represents marine accumulations of mud, silt and sand deposited in the deeper parts of the Late Cretaceous Epicontinental Sea that covered much of the western interior region of North America. Mechanically, Pierre I shale exhibits plastic behaviour, a high sensitivity to moisture content, and is significantly weaker than Tournemire shale (Figure 3). The test matrix includes:

1. A series of unconfined compression tests at different bedding plane orientations (θ = 0°, 30°, 45°, 60°, 90°).
2. A series of drained triaxial compression tests with the bedding planes orientated normal to the axis of the specimen (θ = 0°) and confining pressures of 200, 500, 1000, 2000 psi. (Figure 5).

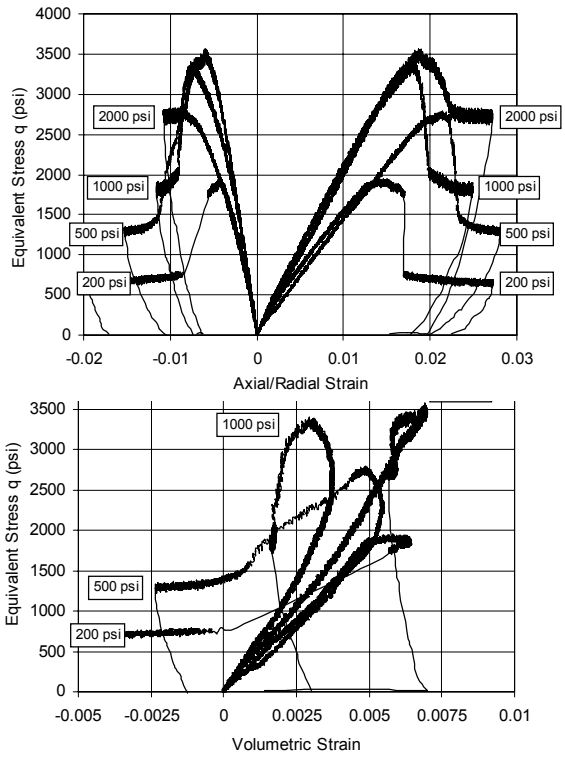

Figure 5. Stress-Strain Curves for Pierre I Shale

The variation of peak stress with bedding plane orientation is shown in Figure 2, where the normalising stress is 2020 psi (Table 1). The collapse load with horizontal bedding planes (θ = 0°) and vertical bedding planes (θ = 90°) are relatively similar, which is consistent with the Tournemire shale. However, unlike the other materials, significant degradation of the collapse strength is only apparent at θ = 45°, with little degradation at θ = 30° and θ = 60°.

The variation of Young's modulus is also consistent with Tournemire shale in that bedding plane closure results in the axial stiffness for the θ = 0° orientation being less than half of the axial stiffness corresponding to θ = 90° (Table 1.)

Orientation θ (°)	*UCS* (*psi*)	*Young's Modulus* (*psi*)	*Poisson's Ratio*
0	2,020	162,500	0.35
30	1,955	178,000	0.39
45	1,301	240,500	0.39
45	1,213	213,600	0.46
60	1,857	231,200	0.39
90	1,929	342,400	0.40

Table 1. UCS Test Results on Pierre I Shale

The conventional triaxial compression (CTC) tests for Pierre I (Figure 5) show that:

1. The Young's modulus stiffens with increasing confining pressure.
2. The peak stress failure surface flattens in the p-q plane with increasing confining pressure.
3. At low confinement the failure is brittle with a sudden loss in strength.
4. Both the magnitude and the rate of strength loss subsequent to the peak load diminish with increasing confinement.
5. The magnitude of the dilatancy in the post-peak regime decreases with increasing confining pressure.

Constitutive Modelling of Shales

The transverse isotropic nature of shales may be represented within a computational model in several ways, including:

1. Inclusion of embedded weakness planes via a smeared or cohesive crack type approach.
2. Direct representation of the planes of weakness as an interface with adhesive, cohesive and frictional properties.
3. Representation of the macroscopically observed deformations using a phenomenological constitutive model based, for example, on orthotropic elastoplasticity.

Whilst each method has advantages and disadvantages this paper focuses on an orthotropic elastoplastic representation as:

1. The material properties may be directly identified from standard experimental test procedures.

2. The model falls within the elastoplastic framework that is well understood in terms of stability and uniqueness, and is extendable to finite strain analysis.

Transverse Isotropic Elasticity

The instantaneous elastic response for an orthotropic material may be defined in the local coordinate system (l) by the generalised Hooke's law as:

$$\boldsymbol{\sigma}_e^l = \boldsymbol{D}_{orth}^l \boldsymbol{\varepsilon}_e^l \tag{1}$$

where $\boldsymbol{D}_{orth}^l$ is a matrix defined by nine material constants, $\boldsymbol{\sigma}_e^l$ is the elastic stress vector, $\boldsymbol{\varepsilon}_e^l$ is the elastic strain vector and superscript l denotes quantities in the local coordinate system aligned with the bedding planes. For transverse isotropic materials the nine elastic constants may be reduced to five:

E_1 - the Young's modulus normal to the bedding plane,
E_2 - the in-plane Young's modulus,
G_{12} - the out-of-plane shear modulus,
ν_{23} - the in-plane Poisson's ratio,
ν_{12} - the out-of-plane Poisson's ratio.

E_1 and ν_{12} are determined from conventional triaxial tests with horizontal bedding planes (θ = 90°) and E_2 and ν_{23} are determined from triaxial tests with vertical bedding planes (θ = 0°). G_{12} may be determined from tests where the bedding planes are non-aligned with the major axes [3] or may be estimated using Saint-Venant's formula [3,10]:

$$\frac{1}{G_{12}} = \frac{1}{E_1} + \frac{1}{E_2} + 2\frac{\nu_{12}}{E_1} \tag{2}$$

In general the elastic response of weak rocks is pressure dependent; Niandou [3] presents a simple empirical law for the evolution of the material parameters with effective mean stress. However, nonlinear elasticity is not considered in this paper.

Transverse Isotropic Elastoplasticity

Shales in general exhibit a clear nonlinear dependence of both the peak strength and post-peak response on the effective mean stress. However, the transition from post-peak dilation to post-peak compression as the confining pressure is increased in triaxial tests is particularly important for weak shales. This transition occurs at confinements sufficiently low to impact, for example, borehole stability predictions, and consequently the constitutive model must be sufficiently rich to accommodate this behaviour. This is in contrast to models derived for moderately strong shales, where yield functions that are open in compression have generally been utilised [13,16]. Inelastic compression, often termed compaction or consolidation, may be represented within a constitutive model by either augmenting a strength criterion, e.g. the Hoffman criterion [14], by a compression cap or by adopting a constitutive law that naturally fulfills the requirement of compressive hardening and shear softening – for example, models founded on critical state soil mechanics. This latter approach is adopted here.

Critical state soil mechanics has developed from experimental measurement of the behaviour clays and sands at large strains, and provides a rational framework that describes strength evolution as a function of the current specific volume. The specific form of an individual critical state model - i.e. the yield surface, flow rule and hardening/softening relationship - is dependent on the nature of the soil, and consequently many differing formulations have been proposed. The Modified Cam Clay model [19] developed for normally consolidated clays under monotonic loading is the earliest model employed computationally. Subsequently many alternative forms have been proposed to accommodate more general stress paths and soil types. The original framework has been, for example, extended to sands [20] and weakly cemented sandstones [21], and the concepts of kinematic hardening, multi-surface plasticity or bounding surface plasticity have been adopted to account for cyclic loading (see [22] for review).

For problems of relevance to petroleum geomechanics, the loading is generally monotonic and consequently the transverse isotropic model is developed by generalising the standard isotropic Modified Cam Clay model.

Isotropic Modified Cam Clay Model

The standard Modified Cam Clay yield function Φ (Figure 6) is defined as:

$$\Phi\left(\boldsymbol{\sigma}, \varepsilon_v^p\right) = \left(\frac{q}{M}\right)^2 + \frac{1}{b^2}(p - p_t + a)^2 - a^2 = 0 \tag{3}$$

where

$$b = \begin{cases} 1 & p \geq (P_t - a) \\ \beta & p < (P_t - a) \end{cases} \tag{4}$$

and

$$a = \frac{1}{1+\beta}(p_t - p_c); \qquad b = \begin{cases} 1 & p \geq (p_t - a) \\ \beta & p < (p_t - a) \end{cases} \tag{5}$$

where p is the effective mean stress, p_t is the tensile intercept, and p_c is the pre-consolidation pressure. The constant M defines the ratio between the two radii of the ellipsoid, which for associated plasticity is the critical state line. β is a material constant that defines the shape of the consolidation cap, and q is the deviatoric effective or equivalent stress defined as:

$$q = \sqrt{3J_2'} = \sqrt{\frac{3}{2}\boldsymbol{S} : \boldsymbol{S}} = \sqrt{\frac{1}{2}\boldsymbol{\sigma}^T \boldsymbol{P} \boldsymbol{\sigma}} \tag{6}$$

where J_2' is the second deviatoric stress invariant, $\boldsymbol{S}$ is the deviatoric stress tensor, $\boldsymbol{\sigma}$ is the stress tensor and $\boldsymbol{P}$ is a projection matrix defined as:

$$\boldsymbol{P} = \begin{bmatrix} \boldsymbol{\Omega} & \boldsymbol{0} \\ \boldsymbol{0} & \boldsymbol{\Gamma} \end{bmatrix}, \ \boldsymbol{\Omega} = \begin{bmatrix} 2 & -1 & -1 \\ -1 & 2 & -1 \\ -1 & -1 & 2 \end{bmatrix}, \ \boldsymbol{\Gamma} = \begin{bmatrix} 6 & 0 & 0 \\ 0 & 6 & 0 \\ 0 & 0 & 6 \end{bmatrix} \tag{7}$$

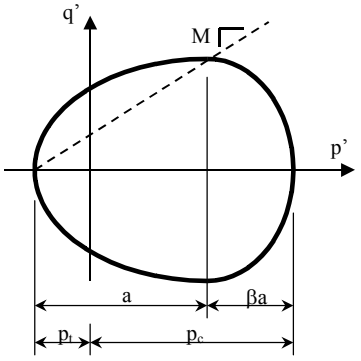

Figure 6. Isotropic Modified Cam Clay Model

The evolution of the yield function is governed by the void ratio or plastic volumetric strain ε_v^p so that:

$$a = a(\varepsilon_v^p) \tag{8}$$

or, more specifically:

$$p_c = p_c(\varepsilon_v^p) \quad \text{and} \quad p_t = p_t(\varepsilon_v^p) \quad . \tag{9}$$

The evolution of the plastic flow is defined by an associated flow rule:

$$\dot{\boldsymbol{\varepsilon}}^p = \dot{\lambda}\frac{\partial F}{\partial \boldsymbol{\sigma}} \tag{10}$$

where the plastic multiplier $\dot{\lambda}$ is consistent with the loading/unloading criterion:

$$\Phi(\boldsymbol{\sigma}, q) \le 0 \qquad \dot{\lambda} \ge 0 \qquad \dot{\lambda}\Phi(\boldsymbol{\sigma}, q) = 0 \tag{11}$$

From the definitions of $\dot{\boldsymbol{\varepsilon}}^p$ and ε_v^p is follows from the plastic flow rule (10) that:

$$\dot{\varepsilon}_v^p = \dot{\lambda}\,\mathrm{tr}\left[\frac{\partial F}{\partial \boldsymbol{\sigma}}\right] \tag{12}$$

Π-Plane Correction for Isotropic Modified Cam Clay

The intersection of the Modified Cam Clay yield surface with the octahedral or π-plane has a circular form (Figure 7). This is contrary to experimental evidence for weakly cemented rocks where the strength observed in reduced triaxial extension (RTE) tests is generally lower than in conventional triaxial compression (CTC) tests. Therefore, whilst the model may be calibrated provide a good fit to CTC tests, it will provide a poor fit to the behaviour in other stress states, e.g. RTE and thick-walled cylinder (TWC) tests and field applications. To overcome this limitation the effective or equivalent stress q is augmented in the yield function with a term $g(\theta_l)$ based on the Lode angle θ_l so that (3) becomes:

$$\Phi\left(\boldsymbol{\sigma}, \varepsilon_v^p\right) = \left(\frac{g(\theta_l)q}{2M}\right)^2 + \frac{1}{b^2}(p - p_t + a)^2 - a^2 = 0 \tag{13}$$

where the Lode angle θ_l is defined as:

$$\theta_l = \frac{1}{3}\sin^{-1}\left[\frac{3\sqrt{3}}{2}\frac{J_3'}{\left(J_2'\right)^{3/2}}\right] \tag{14}$$

where J_3' is the third deviatoric stress invariant.

Several different definitions of the function $g(\theta_l)$ have been proposed in the literature. The definition adopted in this study is:

$$g\left(\theta_l\right) = \left[\left(1+1/\xi\right) - \left(1-1/\xi\right)\sin 3\theta_l\right] \tag{15}$$

where ξ is a constant and must be in the range $0.778 \le \xi \le 1.0$ to ensure convexity of the yield function. This function yields

$$\begin{aligned} \theta &= -30° \qquad \sin 3\theta = -1 \quad t = q/\xi \\ \theta &= 0° \qquad\ \ \sin 3\theta = 0 \quad t = \frac{1}{2}q\left[1+1/\xi\right] \\ \theta &= 30° \qquad \sin 3\theta = 1 \quad t = q \end{aligned} \tag{16}$$

The definition of q in the yield function is, therefore, unchanged for CTC tests so that the material parameters may be calibrated in the usual manner and the value of ξ estimated from RTE or TWC tests.

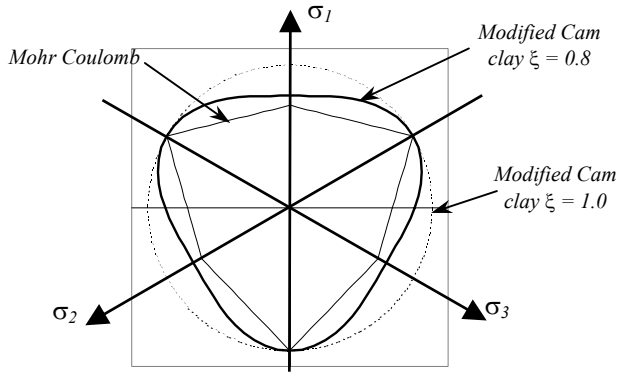

Figure 7. Comparison of Modified Cam Clay, Modified Cam Clay with ξ = 0.8 and Mohr Coulomb yield functions (ϕ=30°).

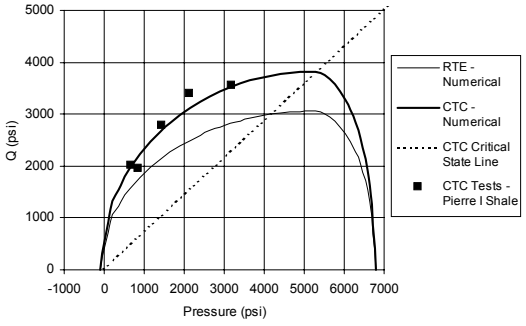

Figure 8. P-Q Representation of Modified Cam Clay (ξ = 0.8)

The π-plane representation shows that the $g(\theta_l)$ correction results in a smooth yield function that approaches shape of the Mohr Coulomb yield function (Figure 7). Note that the strength predicted in RTE tests is still greater than that predicted by the Mohr Coulomb function for the chosen

friction angle of 30°. A fit through all the apex of the Mohr Coulomb surface is only achievable at low values of friction angle, ϕ, because as ϕ increases the Mohr Coulomb yield function becomes increasingly triangular. It should also be noted that the dependence of the yield strength on the Lode angle impacts the concept of the critical state, as the residual friction angle in the RTE test is significantly less than in standard CTC tests.

Extension of the Cam Clay Model for Transverse Orthotropic Materials

The Modified Cam Clay yield function may be extended to orthotropic materials by defining a yield function of the form:

$$\Phi\left(\boldsymbol{\sigma},\varepsilon_v^p\right)=\left(\frac{g(\theta)q_{orth}}{2M}\right)^2+\frac{1}{b^2}(\boldsymbol{p}_{orth}\boldsymbol{\sigma}-p_t+a)^2-a^2=0 \qquad (17)$$

where the isotropic equivalent effective stress has been replaced by an orthotropic function of the form:

$$q_{orth}=\sqrt{\frac{1}{2}\left(\boldsymbol{\sigma}^l\right)^T\boldsymbol{P}_{orth}\boldsymbol{\sigma}^l} \qquad (18)$$

the orthotropic matrices are defined as:

$$\boldsymbol{P}_{orth}=\begin{bmatrix}\boldsymbol{\Omega}_{orth} & \boldsymbol{0}\\ \boldsymbol{0} & \boldsymbol{\Gamma}_{orth}\end{bmatrix} \qquad (19)$$

and $\boldsymbol{\sigma}^l$ is the stress vector aligned with the local material axes defining the principal material directions which is defined as:

$$\boldsymbol{\sigma}^l=\begin{bmatrix}\sigma_x^l & \sigma_y^l & \sigma_z^l & \tau_{xy}^l & \tau_{yz}^l & \tau_{zx}^l\end{bmatrix}^T \qquad (20)$$

$\boldsymbol{P}_{orth}$ and $\boldsymbol{p}_{orth}$ are a matrix and vector of material constants respectively and $\boldsymbol{P}_{orth}$ is taken as identical to the orthotropic model proposed by Hill [9] for metal plasticity. Several different conventions have been adopted to specify the components of $\boldsymbol{P}_{orth}$ and $\boldsymbol{p}_{orth}$ and the magnitude of each cell is independent of the chosen system. Following the system of Hashagen and de Borst [23]:

$$\boldsymbol{\Omega}_{orth}=\begin{bmatrix}2(\alpha_4+\alpha_6) & -2\alpha_4 & -2\alpha_6\\ -2\alpha_4 & 2(\alpha_4+\alpha_5) & -2\alpha_5\\ -2\alpha_6 & -2\alpha_5 & 2(\alpha_5+\alpha_6)\end{bmatrix} \qquad (21)$$

$$\boldsymbol{\Gamma}_{orth}=\begin{bmatrix}6\alpha_7 & 0 & 0\\ 0 & 6\alpha_8 & 0\\ 0 & 0 & 6\alpha_9\end{bmatrix} \qquad (22)$$

$$\boldsymbol{p}_{orth}=\begin{bmatrix}\alpha_1 & \alpha_2 & \alpha_3 & 0 & 0 & 0\end{bmatrix} \qquad (23)$$

and α_1 - α_9 are material parameters.

For transverse isotropic materials where the local π-plane is isotropic, then from [7]:

$$\alpha_4=\alpha_6,\quad \alpha_7=\alpha_9,\quad \alpha_8=\frac{2}{3}(2\alpha_4+\alpha_5) \qquad (24)$$

so that

$$\boldsymbol{\Omega}_{orth}=\begin{bmatrix}4\alpha_4 & -2\alpha_4 & -2\alpha_4\\ -2\alpha_4 & 2(\alpha_4+\alpha_5) & -2\alpha_5\\ -2\alpha_4 & -2\alpha_5 & 2(\alpha_4+\alpha_5)\end{bmatrix} \qquad (25)$$

and

$$\boldsymbol{\Gamma}_{orth}=\begin{bmatrix}6\alpha_7 & 0 & 0\\ 0 & 4(2\alpha_4+\alpha_5) & 0\\ 0 & 0 & 6\alpha_7\end{bmatrix} \qquad (26)$$

This gives three unknown parameters $\alpha_4,\alpha_5,\alpha_7$ that may be determined from a series of triaxial tests with differing bedding plane orientations.

Stress Update Procedure

Considering a time interval [*t*, *t*+Δ*t*] the trial state is determined as:

$$\left(\boldsymbol{\sigma}^l\right)^{Trial}=\boldsymbol{D}_{orth}^l\left(\boldsymbol{\varepsilon}_e^l\right)^{Trial} \qquad (27)$$

If the trial states lies within the elastic domain, i.e. if $\Phi\left[\left(\boldsymbol{\sigma}^l\right)^{Trial},\varepsilon_v^p\right]\le 0$, the trial state corresponds to the actual state at *t*+Δ*t* and the increment is elastic. If the yield function is violated the stress update is defined by:

$$\boldsymbol{\sigma}^{t+\Delta t}=\boldsymbol{\sigma}^{Trial}-\boldsymbol{D}_{orth}\Delta\boldsymbol{\varepsilon}_p \qquad (28)$$

where $\Delta\boldsymbol{\varepsilon}_p=f\left(\boldsymbol{\sigma}^{t+\Delta t},\Delta\lambda\right)$ and the superscript *l* has been dropped for brevity. The yield function (17) may be redefined for convenience as:

$$\Phi=\frac{1}{M^2}(F_1)^2+\frac{1}{b^2}(F_2)^2-a^2=0 \qquad (29)$$

where

$$F_1=\frac{q_{orth}}{2}\mathrm{g}\quad\text{and}\quad F_2=p_{orth}\boldsymbol{\sigma}-p_t+a \qquad (30)$$

A fully implicit backward Euler integration scheme is employed so that, using (10), the incremental flow rule is defined as:

$$\Delta\varepsilon^p=\Delta\lambda\frac{\partial\Phi}{\partial\boldsymbol{\sigma}^{t+\Delta t}}=\Delta\lambda\boldsymbol{N}^{t+\Delta t}\quad\text{and}\quad\dot{\varepsilon}_v^p=\dot{\lambda}\,\mathrm{tr}\left[\boldsymbol{N}^{t+\Delta t}\right] \qquad (31)$$

where N is the flow vector defined by:

$$\boldsymbol{N}=\frac{1}{M^2}\frac{\partial(F_1^2)}{\partial\boldsymbol{\sigma}}+\frac{1}{b^2}\frac{\partial(F_2^2)}{\partial\boldsymbol{\sigma}} \qquad (32)$$

The plastic corrector phase may then be formulated using the requirement that equations (28), (29) and (31) must be satisfied at *t*+Δ*t*. Systems of equations of this type are commonly found for pressure dependent constitutive models and can generally be reduced to a single unknown Δλ. However, in this case additional complexity introduced by the π-plane correction term prevents this simplification. Therefore, an eight-equation system may be defined as:

$$\begin{aligned} \boldsymbol{Y_I} &= \boldsymbol{\sigma}^{t+\Delta t} - \boldsymbol{\sigma}^{trial} + \Delta\lambda \boldsymbol{D}\boldsymbol{N}^{t+\Delta t} \\ Y_2 &= \Delta\varepsilon_v^p - \Delta\lambda \,\mathrm{tr}(\boldsymbol{N}^{t+\Delta t}) \\ Y_3 &= \frac{1}{M^2} F_1^2(\boldsymbol{\sigma}^{t+\Delta t}, \Delta\lambda) + \frac{1}{b^2} F_2{}^2(\boldsymbol{\sigma}^{t+\Delta t}, \Delta\lambda) - a^2(\varepsilon_v^{p\,t+\Delta t}) \end{aligned} \tag{33}$$

where $\boldsymbol{Y}_1$ is a vector of length six and the primary unknowns are the six stress components $\boldsymbol{\sigma}^{t+\Delta t}$, the plastic multiplier $\Delta\lambda$, the incremental volumetric strain $\Delta\varepsilon_v^p$. This system may be solved using Newton-Raphson iteration using:

$$\begin{bmatrix} \frac{\partial \boldsymbol{Y_I}}{\partial \boldsymbol{\sigma}} & \frac{\partial \boldsymbol{Y_I}}{\partial(\Delta\varepsilon_v^p)} & \frac{\partial \boldsymbol{Y_I}}{\partial(\Delta\lambda)} \\ \frac{\partial Y_2}{\partial \boldsymbol{\sigma}} & \frac{\partial Y_2}{\partial(\Delta\varepsilon_v^p)} & \frac{\partial Y_2}{\partial(\Delta\lambda)} \\ \frac{\partial Y_3}{\partial \boldsymbol{\sigma}} & \frac{\partial Y_3}{\partial(\Delta\varepsilon_v^p)} & \frac{\partial Y_3}{\partial(\Delta\lambda)} \end{bmatrix} \begin{Bmatrix} d\boldsymbol{\sigma} \\ d(\Delta\varepsilon_v^p) \\ d(\Delta\lambda) \end{Bmatrix} = (-1) \begin{Bmatrix} \boldsymbol{Y_I} \\ Y_2 \\ Y_3 \end{Bmatrix} \tag{34}$$

The consistent tangent matrix may be derived by taking the variation of the stress update (28) to give:

$$d\boldsymbol{\sigma} = \boldsymbol{D}d\boldsymbol{\varepsilon} - d(\Delta\lambda)\boldsymbol{D}\boldsymbol{N} - \Delta\lambda \boldsymbol{D}d\boldsymbol{N} \tag{35}$$

Noting that:

$$d\boldsymbol{N} = \frac{\partial \boldsymbol{N}}{\partial \boldsymbol{\sigma}} d\boldsymbol{\sigma} + \frac{\partial \boldsymbol{N}}{\partial(\Delta\varepsilon_v^p)} d(\Delta\varepsilon_v^p) \tag{36}$$

and defining $\boldsymbol{c}_1 = [1, 1, 1, 0, 0, 0]$ so that:

$$d(\Delta\varepsilon_v^p) = \boldsymbol{c}_1 \boldsymbol{N} d(\Delta\lambda) + \Delta\lambda \boldsymbol{c}_1 d\boldsymbol{N} \tag{37}$$

Substituting (38) in (36) gives:

$$d\boldsymbol{N} = \boldsymbol{B}\frac{\partial \boldsymbol{N}}{\partial \boldsymbol{\sigma}} d\boldsymbol{\sigma} + (\boldsymbol{c}_1 \boldsymbol{N})\boldsymbol{B}\frac{\partial \boldsymbol{N}}{\partial(\Delta\varepsilon_v^p)} d(\Delta\lambda) \tag{38}$$

where

$$\boldsymbol{B} = \left[\boldsymbol{I} - \Delta\lambda \frac{\partial \boldsymbol{N}}{\partial(\Delta\varepsilon_v^p)} \otimes \boldsymbol{c}_1 \right]^{-1} \tag{39}$$

Substitution of (39) in (35) leads to:

$$d\boldsymbol{\sigma} = \boldsymbol{R}\{d\boldsymbol{\varepsilon} - \bar{\boldsymbol{N}} d(\Delta\lambda)\} \tag{40}$$

where

$$\boldsymbol{R} = \left[I + \Delta\lambda \boldsymbol{D}\boldsymbol{B}\frac{\partial \boldsymbol{N}}{\partial \boldsymbol{\sigma}} \right]^{-1} \boldsymbol{D} \tag{41}$$

and

$$\bar{\boldsymbol{N}} = \boldsymbol{N} + \Delta\lambda \boldsymbol{c}_1 \boldsymbol{N}\boldsymbol{B}\frac{\partial \boldsymbol{N}}{\partial(\Delta\varepsilon_v^p)} \tag{42}$$

Noting that $\Delta\Phi = 0$ so that:

$$d\Phi = \boldsymbol{N} d\boldsymbol{\sigma} + \left(\frac{2F_2}{b^2}\frac{\partial F_2}{\partial(\Delta\varepsilon_v^p)} - 2a\frac{\partial a}{\partial(\Delta\varepsilon_v^p)} \right) d(\Delta\varepsilon_v^p) = 0 \tag{43}$$

which leads to:

$$d(\Delta\lambda) = \frac{\boldsymbol{T}^T \boldsymbol{R} d\boldsymbol{\varepsilon}}{\boldsymbol{T}^T \boldsymbol{R}\bar{\boldsymbol{N}} - A\boldsymbol{c}_1 \boldsymbol{N}} \tag{44}$$

where

$$\boldsymbol{T} = \boldsymbol{N} + A\Delta\lambda \boldsymbol{c}_1 \frac{\partial \boldsymbol{N}}{\partial \boldsymbol{\sigma}} \tag{45}$$

and

$$A = \left(\frac{2F_2}{b^2}\frac{\partial F_2}{\partial(\Delta\varepsilon_v^p)} - 2a\frac{\partial a}{\partial(\Delta\varepsilon_v^p)} \right) \left(1 - \Delta\lambda \boldsymbol{c}_1 \frac{\partial \boldsymbol{N}}{\partial(\Delta\varepsilon_v^p)} \right)^{-1} \tag{46}$$

Then substitution of (44) in (35) gives:

$$d\boldsymbol{\sigma} = \left[\boldsymbol{R} - \frac{\boldsymbol{R}\bar{\boldsymbol{N}}\boldsymbol{T}^T \boldsymbol{R}}{\boldsymbol{T}^T \boldsymbol{R}\bar{\boldsymbol{N}} - A\boldsymbol{c}_1 \boldsymbol{N}} \right] d\boldsymbol{\varepsilon} = \boldsymbol{D}_{ep} d\boldsymbol{\varepsilon} \tag{47}$$

Typically, the principal material directions for structured shales are known *a priori* as the bedding planes are evident by visual inspection. Hence, a specific measure of fabric evolution is not required. However, for the cases of induced anisotropy and bedding plane evolution due to large strains this is no longer true and an evolution law for the fabric tensor must be implemented [17,18]. This issue is not addressed in this paper.

Regularization of the Softening Process

Like all strength based constitutive models, critical state theory alone cannot fully describe the behaviour of typical sandstones and shales as it is based on the concept of homogeneous deformation. More especially, at relatively low mean stress the characteristic deformation of quasi-brittle materials exhibits a transformation from a homogeneous strain field to a heterogeneous strain field with localized regions of intense strain as the load is increased. There is, therefore, a need to invoke constitutive relationships, generically known as regularization methods or localization limiters that naturally introduce a micro-structural length-scale into the formulation. In this study the standard continuum is regularized by incorporation of fracture mechanics concepts.

Fracture energy regularization [24, 25] arises from linear-elastic fracture mechanics theory (LEFM) and has been adopted by numerous researchers for Mode I fracturing of quasi-brittle materials. Generally, the strain-softening constitutive response includes additional material constants associated with the crack band width $l_c^{(m)}$ that is the characteristic length for the material; e.g. the grain size. Whilst the standard fracture energy approach has been shown to work well for Mode I fracturing of rock and concrete, the characteristic response of some rock types shows significant departure from the assumptions of LEFM. This may be approximately described by assuming that the energy release rate for fracture growth is variable and is defined by a nonlinear resistance curve [24] instead of the constant G_f. Adoption of this concept leads to a simple extension of the frictional regularization model of Pietruszczak and Mróz [25]

whereby the scalar inelastic strain measure $\tilde{\varepsilon}_{inel}$ that identifies the evolution of the state variables is defined as:

$$\tilde{\varepsilon}_{inel}^{(e)} = \tilde{\varepsilon}_{inel}^{(m)} \left[\frac{l_c^{(m)}}{l_c^{(e)}} \right]^n \tag{48}$$

where the exponent n is a material constant and superscripts m and e refer to the reference material and element respectively.

The fracture energy approach has the following advantages:

1. The observed size effect dependence of the collapse load on structure size is obtained.
2. Mesh invariance of the global energy dissipation is maintained.
3. The approach may be implemented to regularize both Mode I and Mode II localization.
4. It is relatively straightforward to implement within any finite strain framework and for a range of constitutive models.

It should be recognized, however, that although the energy dissipation is mesh independent the localization limiter is strictly only valid provided $l_c^{(e)} \geq l_c^{(m)}$; i.e. if the localization bandwidth is less than or equal to the element characteristic length so that localization occurs in a band of one element width. For practical field simulations this limitation is of little consequence [27]. The efficacy of this methodology has been previously demonstrated [27] by simulation of TWC tests on Berea and Castlegate sandstones, where the predicted dependence of the collapse pressure on the specimen size is in good agreement with the experimental data.

Calibration of the Constitutive Model

The material parameters for the orthotropic elastoplastic model are calibrated by back-analysis of uniaxial and triaxial tests (Figure 9), with the drained triaxial tests being represented by an initial hydrostatic compression stage followed by further axial displacement. A 3D multi-element representation of the specimen using half symmetry model discretised using 4500 hexahedral elements is utilised. This is in contrast to the commonly used approach of calibrating material parameters by matching the stress-strain curves using a single point or single element representation. The multi-element approach is essential to accommodate the non-uniform deformation induced by the bedding planes, end effects and the localised displacements on shear bands subsequent to the peak load.

The elastic properties may be determined directly from the linear part of the stress-strain curves at different angles. For the current case the elastic properties are identified using the UCS tests (Table 1). Note, however, that UCS tests are not ideal for identification of elastic constants, and Poisson's ratio in particular, as the experimental scatter in low confinement tests is quite large. Therefore, extra weight was placed on the triaxial data for identification of ν_{23} and ν_{12}. G_{12} was determined using Saint-Venant's formula (Equation (2)).

E_1 (psi)	E_2 (psi)	G_{12} (psi)	ν_{12}	ν_{23}
200,000	342,400	89,900	0.32	0.32

Table 2. Elastic Material Parameters

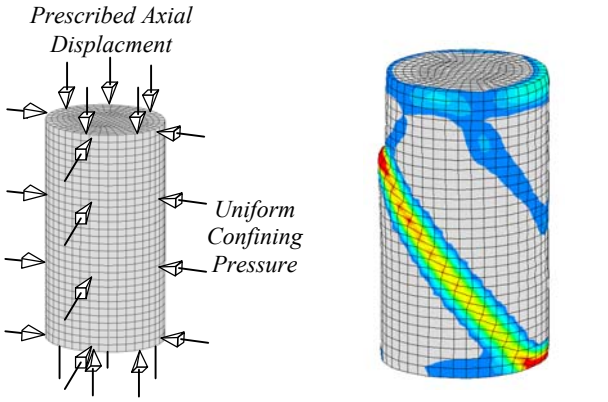

(a) Mesh Discretisation (b) Post-Peak Configuration Showing Shear Band

Figure 9. Model for Triaxial Tests

The initial peak surface is chosen using the peak values from the uniaxial and triaxial experiments at $\theta = 0°$ (Figure 10) and by performing a stress-dilatancy analysis of the experimental data. The stress-dilatancy plot is used to identify the residual friction at constant volume deformation ($d\varepsilon_v = 0$) that corresponds to the parameter M. Insufficient data is available to identify the shape of the yield surface in the compressive region and β is set from previous experience with sandstones.

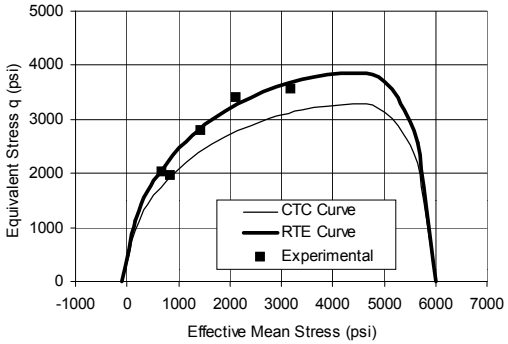

Figure 10. Yield Surface (θ=0°) in the p-q Plane

P_c	P_t	M	β
6000	-50	0.83	0.3

Table 3. Material Parameters Defining Yield Surface in p-q Plane

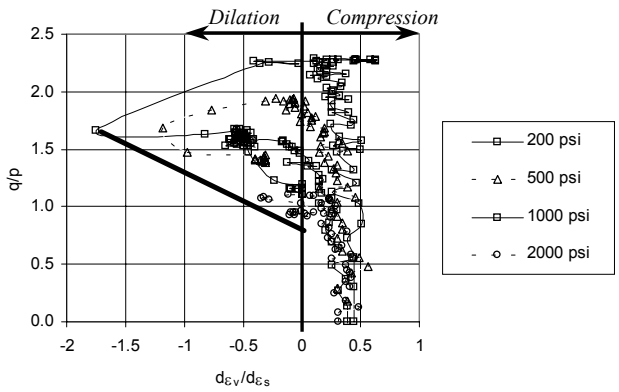

Figure 11. Stress-Dilatancy Analysis of the Triaxial Experimental Data

The yield surface is assumed to be centred on the hydrostatic axis ($\alpha_1 = \alpha_2 = \alpha_2 = 1/3$) and the three material constants defining the elliptical shape of the yield function in the π-plane are then evaluated by back-analysis of the UCS tests at different bedding plane orientations (Figure 12). The model is calibrated to fit the experiments at $\theta = 0°$, $\theta = 45°$ and $\theta = 90°$, but the smooth variation of peak stress predicted by the model under-estimates the experimentally observed values at $\theta = 30°$ and $\theta = 60°$. As pointed out earlier, however, the high experimental values at $\theta = 30°$ and $\theta = 60°$ are not typical of other published data on shales which exhibit a much smoother variation in strength with θ (Figure 2). The nine orthotropic elastoplastic constants are provided in Table 4.

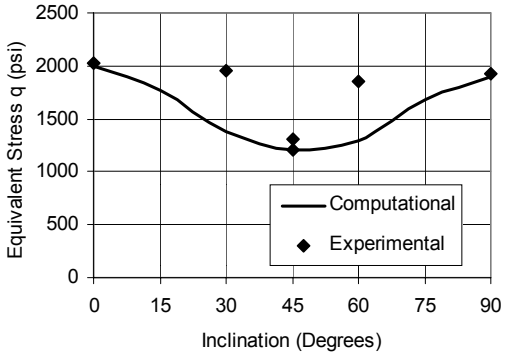

Figure 12. Variation of Failure Stress for Pierre 1 Shale with Bedding Plane Orientation in UCS Tests

Constant	Value	Constant	Value	Constant	Value
α_1	0.333	α_4	0.47	α_7	1.02
α_2	0.333	α_5	0.53	α_8	2.0
α_3	0.333	α_6	0.47	α_9	2.0

Table 4. Orthotropic Yield Surface Material Parameters

The post peak softening and regularization parameters are then evaluated by back-analysis of the triaxial tests. The characteristic length scale is set at 0.05" and the evolution of the tensile intercept and the pre-consolidation pressure is represented by a piecewise linear function (Table 5). The stress-strain response for the final characterisation provides a good approximation to the experimentally observed response (Figure 13).

ε_v^p	P_c (psi)	P_t (psi)
0.00	6000	-50
0.04	2000	-1
0.10	100	-1

Table 5. Evolution of Material Parameters

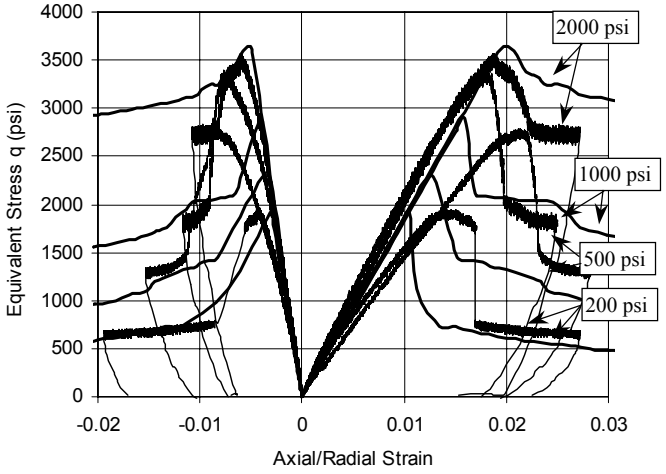

Figure 13. Comparison of Numerical and Experimental Predictions for Triaxial Tests on Pierre I Shale

Conclusions

The behaviour of shale is complex due to its laminated structure and strength degradation subsequent to attainment of the peak load. These issues pose a serious challenge to computational modelling and important aspects of the experimentally observed deformation of weak shales that should be represented in a constitutive model are:

1. The variation of elasticity and compressive strength with the angle between the bedding planes and loading direction, the Young's modulus normal to the bedding planes being lower than the Young's modulus in the plane of the bedding.
2. The nonlinear failure surface in the p-q plane.
3. The brittle shear failure and subsequent strength loss at low confining pressures.
4. The hardening of the failure surface due to consolidation at higher confining pressures.

An orthotropic elastoplastic model, formulated by generalising the Modified Cam Clay model for orthotropic media is presented and it is shown that this model is able to represent the principal characteristics of weak shales described above.

A regularization procedure is also presented that ensures mesh invariance and correctly reproduces the dependence of strength on the size of the test specimen.

Calibration of the model parameters is discussed and the model is validated by comparison with the results of uniaxial and triaxial compression tests for a weak shale performed at different orientations to bedding planes.

The current research is ongoing and the applications to model the deformation and failure of small- and large-scale thick-walled cylinder tests with differing bedding plane orientations, as well as extensions of this analysis to address problems of borehole instability, will be presented in subsequent publications.

Acknowledgement

The authors wish to thank BP America Inc. for permission to publish this paper. TerraTek Inc. of Salt Lake City, Utah, is acknowledged for undertaking the experimental testing of the Pierre 1 Shale reported here.

References

1. Attewell, B., Sandford, M.R., Intrinsic shear strength of a brittle anisotropic rock I. Experimental and mechanical interpretation, Int. J. Rock Mech Min. Sci., Vol. 11, 423-451, 1974.
2. Donath, F.A., Strength variation and deformational behaviour in anisotropic rock., In "State of stress in the Earth's crust", eds. W.R.Judd, Elsevier, 281-297, 1964.
3. Niandou, H. *et al.* "Laboratory Investigation of the Mechanical Behaviour of Tournemire Shale", Int. J. Rock Mech. Min. sci., Vol.34, No.1, 3-15, 1997.
4. Duveau, G., Shao, J.F., Henry, J.P., Assessment of some failure criteria for strongly anisotropic rock, Mech. Frict. Cohesive Mater., Vol.3, 1-26, 1998
5. Jaeger, J.C., Shear failure in anisotropic rocks, Geol. Mag., Vol..97, 65-72, 1960.
6. McLamore, R., Gray, K.E., The mechanical behaviour of anisotropic sedimentary rocks, J. Eng. Ind., Trans. Of the ASME, Vol.89, 62-73, 1967.
7. Tsai, S.M., Wu, E., A general theory of strength of anisotropic materials, J. Composite Mater., Vol.5, 58-80, 1971.
8. Pariseau, W.G., Plastic theory for anisotropic rocks and soils, In "Proceedings of the tenth Symposium on Rock Mechanics", AIME, 267-295, 1972.
9. Hill, R., A theory of yielding and plastic flow of anisotropic metals, In "Proceedings of the Royal Society", London, Vol.193, 281-297, 1948.
10. Ong, S.H., Roegiers, J-C., Horizontal wellore collapse in an anisotropic formation, SPE 25504, 1993.
11. Nova, R., The failure of transversely anisotropic rocks in triaxial compression, Int. J. Rock Mech Min. Sci., Vol.17, 325-332, 1980.
12. Nova, R., Zaninetti, A., An investigation into the tensile behaviour of a schistose rock, Int. J. Rock Mech Min. Sci., Vol.27, 231-242, 1990.
13. Cazacu, O., Critescu, N.D., A paraboloid failure surface for transversely isotropic materials, Mech. Materials, Vol. 31, 381-393, 1999.
14. Hoffman, O., The brittle strength of orthotropic materials, J Composite Mater., Vol.1, 200-206, 1967.
15. Koh, C.G., Owen, D.R.J., Peric, D., Explicit dynamic analysis of elasto-plastic laminated composite shells: implementation of non-iterative stress update schemes for the HOFFMAN yield criterion., Computational Mechanics, Vol.16, 307-314, 1995.
16. Pietruszczak, S., Lydzba,D., Shao, J.F., Modelling of inherent anisotropy in sedimentary rocks, Int. J. Solids Struct., Vol.39, 637-648, 2002.
17. Dafalias, Y.F., An anisotropic critical state clay plasticity model, in "Constitutive laws for engineering materials: Theory and applications", C.S. Desai et al., eds, 513-521, 1987.
18. Voyiadjis, G.Z., Song, C.R., Finite strain, anisotropic modified Cam Clay Model with Plastic Spin I: Theory, J. Eng. Mech., 1012-1019, October, 2000.
19. Roscoe, K.H., Burland, J.B., On the generalised stress-strain behaviour of wet clays, In "Engineering Plasticity", eds. J.Heyman, F.A.Leckie, 535-609, Cambridge University Press, 1968.
20. Been, K., Jefferies, M.G., Hachey, J.E., The critical state of sands, Geotechnique, Vol.41, 365-381, 1991.
21. Coop, M.R., The mechanics of uncemented carbonate sands, Geotechnique, Vol.40, 607-626, 1990.
22. Manzari, M.T., Dafalias, Y.F., A critical state two-surface plasticity model for sands, Geotechnique, Vol.47, 255-272, 1997
23. Hashagen, F., de Borst, R., Enhancement of the Hoffman criterion with an anisotropic hardening model, Computers and Structures, Vol.79, 637-651, 2001.
24. Bažant, Z.P., Oh, B., Crack band theory for fracture of concrete, RILEM, Materials and Structures, Vol. 16, pp.155-177, 1983.
25. Pietruszczak, S., Mróz, Z., Finite element analysis of deformation of strain softening materials. Int. J. Num. Meth. Eng., Vol. 17, pp. 327-334, 1981.
26. Vardoulakis, I., Sulem, J., 1995. Bifurcation analysis in geomechanics. Blackie Academic & Professional, London.
27. Crook, T., Willson, S.M, Yu, J.G., Owen, R., Computational Modelling of the Localized Deformation Associated with Borehole Breakout in Quasi-Brittle Materials, J. Petr. Sci. Eng., in press.